*To appear in Int. J. Impact Engineering (2009)*

# A study of inclined impact in polymethylmethacrylate plates

Dorogoy[(1)] A., Rittel[(1*)] D. and Brill[(2)] A.

[(1)] *Faculty of Mechanical Engineering, Technion – Israel Institute of Technology, 32000 , Haifa, Israel.*

[(2)] *RAFAEL, P.O. Box 2250, Haifa, Israel.*

**Abstract**

The penetration and perforation of a polymethylmethacrylate (PMMA) plate is investigated experimentally and numerically. Two combined failure criteria are used in the numerical analyses: ductile failure with damage evolution and tensile failure. The measured mechanical properties of PMMA are input to the analysis. The determination of the damage evolution parameter in this material is calibrated by simulating and replicating shear localization results obtained in confined PMMA cylinders. The numerical simulation based on these parameters is tested by comparing the numerical trajectory prediction to actual trajectories of inclined impacts of projectiles. The first comparison is qualitative and shows that the numerical simulation predicts ricochet of a projectile impacting at an angle of inclination $30^o$ as in Rosenberg et al. [1]. An additional successful comparison with experimental results of inclined impact of a 0.5" AP projectile on 3 PMMA plates is reported. The contribution of each failure criterion to the projectile trajectory is studied, showing that the ductile failure criterion enforces a straight trajectory in the initial velocity direction while the tensile failure criterion controls the deflection and ricochet phenomenon. The numerical analyses are further used to study the effect of the angle of inclination on the trajectory and kinetic energy of the projectile. It is found that the ricochet phenomenon happens for angles of inclination of $0^\circ < \alpha \le 30^\circ$. The projectile perforates the plate for $50^\circ \le \alpha \le 90^\circ$, thus defining a failure envelope for this experimental configuration . For normal impact ($\alpha=90^o$) the depth of penetration scales linearly with the projectile's mass and can be fitted by a quadratic function of the impact velocity.

(*) Corresponding author: *merittel@technion.ac.il*

## 1. Introduction

The impact and perforation of polymethylmethacrylate (PMMA) plates has been the subject of recent investigations by Rosenberg et al. [1] who showed an interesting ricochet phenomenon that occurs for inclined impacts. These authors presented an extensive experimental and numerical study, with the main conclusion that spalling (dynamic tensile failure) is indeed the governing factor in the generation of the ricochet. In [1], the actual mechanical properties of PMMA were not characterized separately, but were systematically varied until a satisfactory similarity between the experiments and the simulations was obtained. More recently, the mechanical properties of polymers at high strain-rates and confinement were investigated: PMMA by Rittel and Brill [2], and polycarbonate (PC) by Rittel and Dorogoy [3]. The influence of the confinement on the mechanical response of these materials was determined. A simple dynamic pressure-sensitive constitutive equation was identified, and it was also observed (Rittel and Brill [2]) that under a suitable confinement level and strain-rate, PMMA can undergo a brittle-ductile transition resulting in the formation of an adiabatic shear band.

It is therefore evident that aside from a brittle (spalling) failure mechanism, PMMA can also undergo ductile deformations (including localized). The extent to which plasticity plays a role in the slant impact/perforation process remains to be investigated. Consequently, this paper addresses the impact and perforation of PMMA plates under the combined effects of brittle spalling and ductile deformations. The investigation is done essentially by numerical simulations into which the ductile and the brittle response of this material are included, along with a comparison to a set of experiments aimed at validating the simulations. The paper is organized in the following way: the numerical details which include the failure criteria, material and failure properties are detailed in section 2. Two experimental verification problems are discussed in section 3. The successful verification of section 3 is followed in sections 4, 5 and 6 by a systematic investigation of the inclined impact of a 0.3" projectile on a PMMA plate. This investigation includes the characterization of the effect of each failure criterion, angle of penetration as

well as the maximum depth of penetration. The paper ends with a discussion and conclusions section.

## 2. Numerical simulations

The numerical simulations were carried out using Abaqus-explicit finite element code [4]. Specific modeling details are outlined next.

### 2.1 Failure criteria

Two failure criteria which are available in Abaqus explicit [4] were used: 1. tensile failure. 2. ductile failure with damage evolution, as discussed next. The failure criteria can be applied separately or combined without any need for a user subroutine.

*2.1.1 Tensile failure [4]*

The "tensile failure" uses the hydrostatic pressure as a measure of the failure stress to model dynamic spall, or a pressure cutoff. It is designed for high-strain-rate deformation and offers a number of choices to model failure. Five failure choices are offered for the failed material points: the default choice, which includes element removal, and four different spall models (the crumbling of a material). These choices are detailed in the chapter 19.2.8 named Dynamic failure models in Abaqus User's Manual. We use the default choice in which when the tensile failure criterion is met at an element integration point, the material point fails and the element is removed. This criterion can be used in conjunction with other failure criteria. It means that for each material point, each failure criterion is verified separately.

*2.1.2 Ductile failure[4]*

The "ductile failure" criterion is used to predict the onset of damage due to nucleation, growth and coalescence of voids. The model assumes that the equivalent plastic strain at the onset of damage $\bar{\varepsilon}_D^{pl}$ is a function of the stress triaxiality ($\eta$) and plastic strain rate ($\dot{\bar{\varepsilon}}^{pl}$), $\bar{\varepsilon}_D^{pl}\left(\eta\ ,\ \dot{\bar{\varepsilon}}^{pl}\right)$. The stress triaxiality is given by $\eta = -p/q$, where $p$ is the hydrostatic pressure, $q$ is the Mises equivalent stress, and $\dot{\bar{\varepsilon}}^{pl}$ is the equivalent plastic strain rate. The damage variable,

$\omega_D = \int \frac{d\bar{\varepsilon}^{pl}}{\bar{\varepsilon}_D^{pl}\left(\eta, \dot{\bar{\varepsilon}}^{pl}\right)}$, increases monotonically with plastic deformation. At each increment during the analysis the incremental growth in $\omega_D$ is computed as $\Delta\omega_D = \frac{\Delta\bar{\varepsilon}^{pl}}{\bar{\varepsilon}_D^{pl}\left(\eta, \dot{\bar{\varepsilon}}^{pl}\right)} \geq 0$. The criterion for damage initiation is met when $\omega_D = 1$. The way the material behaves after initiation until final failure is defined by "damage evolution", as discussed next.

### *2.1.3 Damage evolution [4]*

Damage evolution is specified in terms of a mesh independent constant such as an equivalent plastic displacement $\bar{u}_f^p$ at the point of failure. The criterion assumes that damage is characterized by a linear progressive degradation of the material stiffness, leading to final failure. Once the damage initiation criterion has been reached, the effective plastic displacement, $\bar{u}^{pl}$, is defined with the evolution equation $\dot{\bar{u}}^{pl} = L\dot{\bar{\varepsilon}}^{pl}$, where $L$ is the characteristic length of the element. The damage variable D increases according to $\dot{D} = \frac{\dot{\bar{u}}^{pl}}{\bar{u}_f^{pl}}$. This definition ensures that when the effective plastic displacement reaches the value $\bar{u}^{pl} = \bar{u}_f^{pl}$, the material stiffness will be fully degraded as D = 1. At any given time during the analysis, the stress tensor in the material is given by the scalar damage equation, $\sigma = (1 - D)\bar{\sigma}$, where $D$ is the overall damage variable and $\sigma$ is the effective stress tensor computed in the current increment. The tensor $\bar{\sigma}$ represents the stresses that would exist in the material in the absence of damage. By default, an element is removed from the mesh if all of the section points at any one integration location have lost their load-carrying capacity.

## 2.2. Polymethylmethacrylate (PMMA) properties

### *2.2.1 Elastic and plastic properties*

The material properties of commercial PMMA were previously investigated by Rittel and Brill [2]. PMMA is assumed to obey the Drucker-Prager material model, with dynamic elastic properties (from [5]) ( $E,\nu$ ), density ( $\rho$ ) and pressure sensitivity ( $\beta$ ) all listed in table 1. Experimentally uniaxial determined stress-plastic strain curves at different strain rates ( $\dot{\varepsilon}=0.0001,1,2000\,\text{and}\,4000\,\text{s}^{-1}$ ) are shown in figure 1. Higher strain rates are not really experienced in the typical perforation tests, so that at this stage the mechanical response of PMMA will be assumed to be similar to that measured at 4000 $s^{-1}$ for higher strain rates, if any.

### *2.3 Failure properties*

#### 2.3.1 Tensile brittle failure

Polymethylmethacrylate is known to be extremely brittle at high strain rates, with a typical spall strength of 100–150 MPa [1, 6]. A representative value of 133 MPa is used throughout this work.

#### 2.3.2 Ductile failure

Maximum plastic strains at which failure initiates as a function of strain rate and triaxiality are listed in table 2. The data is taken from [2], and "all" means that numerically, the triaxiality $\eta$ could range $-100 \le \eta \le 100$.

#### *2.3.3 Calibration of damage evolution parameter $\bar{u}_f^{pl}$*

Transient axisymmetric numerical analyses were performed with Abaqus 6.7 [4] in order to determine the damage evolution constant $\bar{u}_f^{pl}$. The experimental results of confined cylinders obtained by Rittel and Brill [2] were simulated numerically using the Drucker-Prager material model and the properties listed in tables 1 and 2 and figure 1. The experimental velocities (which were ~25 m/s) were applied. The numerical details of the simulations are fully described in Rittel and Dorogoy [3]. The formation of a conical plug was observed in [2], which is indicative of adiabatic shear failure, for a given range of strain rates and confining pressures. Different values of $\bar{u}_f^{pl}$ were tested numerically until this experimental typical failure mode was reproduced. A value of $\bar{u}_f^{pl} = 80\,\mu m$ was thus determined.

The numerical evolution of the damage is shown in figure 3 at times 51, 55 and 59 μs. The time origin is taken from the arrival of the stress wave to the upper face of the adapter pressing the confined specimen [2]. It can be observed that a conical plug is created at t = 59 μs. The contour maps show the equivalent plastic strain.

## 3. Experimental verification of numerical results

Two test cases for which experimental results are available are chosen for the verification and validation of the numerical results. The first case involves a $30^{\circ}$ inclined impact of a 0.3" projectile onto a 50 mm thick PMMA plate [1]. The verification consists of a numerical replication of the observed ricochet phenomenon. The second test case involves a $30^{\circ}$ inclined impact of a 0.5" projectile on a combination of 3 layered 27-45 mm thick PMMA plates.

### *3.1 A 30° inclined impact of 0.3" projectile on a PMMA plate*

The 0.3" projectile is shown in figure 4a. The projectile is assumed to be made of steel with a density $\rho = 7800\ Kg/m^3$, Young's modulus $E = 210\ GPa$ and Poisson's ratio $\nu = 0.3$. To avoid erosion no plastic deformation is assumed. The 5.8 gr projectile impacts a PMMA plate at a velocity $V = 720\ m/\sec$ with an angle of inclination $\alpha = 30^{\circ}$ as seen in figure 4b.

The PMMA plate is 250 mm long, 50 mm high and 80 mm wide [1]. The material properties of section 3 were used here with one exception. The plate is modeled as a strain rate dependent elastic-plastic von Mises material. This is similar to using the Drucker-Prager (DP) material model with $\beta = 0$. The reason for this simplification is that the tensile failure criterion of Abaqus is not available with the DP model. In Rittel and Dorogoy [3], the effect of $\beta$ on the pressure and the von Mises equivalent stress of a confined DP material was studied. It was shown that $\beta$ has a minor influence on the pressure, so that the assumption of Mises plasticity ( $\beta = 0$ ) will not significantly affect the tensile failure criterion. Yet, one should note that this assumption contributes to a slightly reduced failure stress which would otherwise be increased by the hydrostatic pressure contribution. Because of the symmetry of the problem, only one half of the plate and projectile are modeled. The mesh of the projectile is made of

1045 elements of type C3D4 which are 4-node linear tetrahedra. The plate is meshed with 25398 elements of type C3D8R which are 8-node linear bricks with reduced integration and hourglass control. A detail showing the mesh of the projectile in comparison to the mesh of the plate is given in figure 5.

The general contact algorithm of Abaqus [4] is used with element-based surfaces which can adapt to the exposed surfaces of the current non-failed elements. Abaqus' frictionless tangential behavior with the penalty formulation is adopted. The contact domain option for first contact is "All* with self". All the surfaces that may become exposed during the analysis, including faces that are originally in the interior of bodies are included in the contact model. We have included all the elements of the plate and projectile in the contact domain since the projectile trajectory is not known *a-priory*. The inclusion requires the use of the INTERIOR face identifier on the data line of the *SURFACE option of Abaqus. The NODAL EROSION parameter is set to NO on the *CONTACT CONTROLS ASSIGNMENT option (which corresponds to the default setting), so contact nodes still take part in the contact calculations even after all of the surrounding elements have failed. These nodes act as free-floating point masses that can experience contact with the active contact faces. The combined failure criteria "tensile failure" and "ductile failure" with "damage evolution" are employed. The numerical trajectory of the projectile is shown in figure 6a together with the experimental result of Rosenberg *et al.* [1] in figure 6b. It can be observed that the numerical results reproduce quite faithfully the experimentally observed ricochet of the projectile.

### *3.2 A 30° inclined impact of 0.5" projectile on 3 PMMA plates*

A 0.5" projectile is shown in figure 7a. The projectile is assumed to be made of steel, as before. To avoid erosion no plastic deformation of the projectile is assumed. The projectile impacts 3 PMMA plates at a velocity $V = 920\ m/\sec$ at an angle of inclination $\alpha = 30^\circ$ as shown in figure 7b.

The dimensions of the PMMA plates are shown in figure 7b. The width of the plates is 82 mm. Such a configuration was tested experimentally in the National Ballistic Laboratory, and the numerical projectile trajectory can thus be compared to the experimental one. The same material properties failure criteria and contact algorithm

which were used in section 3.1 are used here. A typical mesh is shown in figure 8. The mesh of the projectile is made of 1488 elements. 3220 elements have been generated for the upper plate, 5320 for the middle plate, and 5500 elements for the bottom plate.

In the experiments, 3 flash X-ray pictures were taken to monitor the trajectory of the projectile within the PMMA plates. Typical results are shown in figure 9 which is comprised of three photos taken at time 980, 1200 and 1400 μs. The first time interval is thus 220 μs while the second is 200 μs. In the first picture the projectile is still horizontal, just touching the middle plate. After 220 μs the projectile emerges out of the middle plate with an inclination angle. In the third picture, the projectile is located outside the plates at a lower angle of inclination compared to the second position.

The numerical trajectory of the projectile within the PMMA plate is shown in figure 10 for three time intervals which correspond to the time intervals of the experimental results of figure 9. In figure 10a, the projectile is seen at time 80 μs when it just touches the middle plate. In figure 3b the projectile is seen at time 300 μs which corresponds to the first 220 μs time interval in the experimental results. In 10c the projectile is shown at 500 μs, corresponding to the next 200 μs in the experimental results of figure 9. Overall, one can note the large resemblance in the position and orientation of the projectile between the experimental and the numerical results.

The two failure criteria which are used in the numerical analysis can fairly well reproduce the penetration and perforation as well as the ricochet trajectory of the projectile. The damaged areas of the PMMA plates are less accurately modeled. A third, fracture mechanics-based criterion, which would be combined to the other two might improve the fragmentation behavior of the PMMA plates, but this would imply the determination of additional material parameters.

## 4. Effect of each failure criterion on the projectile trajectory

The trajectory of the projectile within the PMMA plate, as shown in figure 6a, is due to the combined effects of the two failure criteria: tensile failure and ductile failure with damage evolution. The problem of section 3.1 was solved two more times, each time with a different failure criterion (instead of applying the combined effect of both failure criteria). The first solution used only the ductile failure criterion with damage

evolution. The second solution used only the tensile failure criterion. All other parameters remained unchanged. In the first solution, the projectile penetrates the plate and continues straight ahead until it stops as shown in figure 11a. For the second solution, the projectile initially penetrates and then changes its direction with a ricochet out of the plate as shown in figure 11b.

It can be observed that the two failure criteria contribute to the overall trajectory of the projectile shown in figure 6a. The ductile failure alone does not contribute to the ricochet phenomenon, as does the tensile failure because of the brittleness of the PMMA (133 MPa). Using only the tensile failure criterion as in [1] causes ricochet, but little penetration. It can be concluded that the addition of the ductile failure criterion is needed to properly reproduce the depth of penetration while the brittle failure criterion will induce the observed ricochet.

## 5. The trajectory of a 0.3" projectile impacting a PMMA plate - effect of the angle of inclination

Predictive simulations of a 5.8 gr, 0.3" steel projectile impacting a PMMA plate with a velocity of 720 m/s, were carried out at different angles of inclination $(\alpha)$. The geometry, material properties, failure criteria properties, mesh and boundary conditions are those described in section 3.1. Nine angles of inclination were considered: $10^o$, $20^o$, $30^o$, $40^o$, $50^o$, $60^o$, $70^o$, $80^o$ and $90^o$. The goal of these simulations is to predict the performance envelope of the PMMA plate in typical impact experiments. The trajectories are shown in figure 12 a-i.

It can be observed that for angles $\alpha \le 40^\circ$, the projectile does not perforate the plate, and for $\alpha \le 30^\circ$ a ricochet is observed. For angles $\alpha \ge 50^\circ$ the projectile fully perforates the plate. The brittleness of the PMMA which manifests itself through the tensile failure criterion is causing the curved trajectory. For angles $\alpha = 50^\circ, 60^\circ$ and $70^\circ$, the initial vertical component of velocity is already high and the ductile failure criterion causes a deep straight penetration. It can be observed that the tensile failure criterion starts to cause rotation of the projectile but this happens relatively (too) late, and the projectile fully perforates the plate, while exiting with a rotational velocity. A wider damaged zone appears at the exit location. For angles $\alpha = 80^\circ$ and $90^\circ$ the

trajectory is a straight line since the initial vertical components of velocities are high and the projectile perforates the plate because the tensile failure effect is not influential enough to alter its direction.

The evolution of the kinetic energy of the projectile for each $\alpha$ is shown in figure 13. The energy is normalized by the initial kinetic energy of the projectile before impact. At $\alpha = 10^\circ$, the plate is slightly damaged, as can be observed in figure 12a and the projectile looses just 6% of its initial kinetic energy. At $\alpha = 20^\circ$ the trajectory within the plate is longer and the projectile looses 92% of its initial kinetic energy before it ricochets out of the plate. At $\alpha = 30^\circ$ the projectile still ricochets, but does so with a very low velocity, and it basically looses ~98% of its initial energy. At $\alpha = 40^\circ$ the projectile comes to a halt within the plate and hence looses 100% of its initial kinetic energy. For $\alpha = 50^\circ$, $60^o$, $70^o$, $80^o$ and $90^o$ the projectile perforates the plate and exits with 24%, 28%, 36%, 50% and 50% respectively of its initial kinetic energy. Since the trajectories of $80^o$ and $90^o$ are very similar their ~50% energy loss is similar. The temporal variation of the kinetic energy (figure 13) is almost linear for all angles of inclination. This indicates that the loss of kinetic energy of the projectile may be approximated by a constant energy loss rate (as a first approximation).

## 6. The maximum depth of penetration (DOP)

The effect of the velocity on the depth of penetration was studied by performing six numerical analyses at six different impact velocities: 200, 300, 400, 500, 600 and 720 m/s. In order to investigate the effect of the mass of the projectile on the DOP, three different densities were assumed in the analyses: $\rho_1 = 7800$, $\rho_2 = 5850$ and $\rho_3 = 3900$ $\left[Kg/m^3\right]$. The PMMA plate is 250 mm long, 150 mm thickand 80 mm wide. Because of symmetry, only one quarter of the physical domain is modeled. A typical model is shown in figure 14 for penetration of a steel projectile impacting the plate at 600 m/s. The results of the corresponding DOP are listed in table 3 and plotted in figure 15. The lines represent the DOP quadratic approximation: $DOP(V_i) = aV_i + bV_i^2 \ \ [m]$ and the dots represent the numerical values of table 3. The coefficients a and b and the coefficient of correlation ($r^2$) are

listed in table 4. The results shown in table 5 indicate that the DOP is a linear function of the density (mass) of the projectile, as evidenced from the similar ratios obtained between densities and DOP's for each case, within the investigated ratios.

The kinetic energy of the projectile versus time for impact velocities: 200, 300, 400, 500, 600 and 720 m/s is plotted in figure 16. Figures 16a, b are for $\rho = 7800\ Kg/m^3$ and figures 16 c, d are for $\rho = 3900\ Kg/m^3$. It can be observed in figure 16a that for 720 m/s the plate is perforated. Figures 16b and 16d are the normalized values of 16a and 16c respectively. The kinetic energy $(E_k)$ is normalized by the initial kinetic energy $(E_k^i)$, and the time (t) is normalized by the time needed to bring the projectile to a halt ($t_{final}$) . The data of impact velocity of 720 m/s is omitted from 16b since the projectile perforates the plate. Figures 16b and 16d show that the lines for the different velocities can be approximated by a "master curve" of the type: $\frac{E_k}{E_k^i} = f\left(\frac{t}{t_f}\right)$. A simple first order approximation might be a linear one.

## 7. Summary and Discussion

This paper presents an investigation of the perforation of PMMA plates under ballistic impact, a subject that was studied in detail by Rosenberg et al. [1]. However, the present study adds a detailed characterization of the contribution of two failure modes, namely the ductile and spalling modes. The ductile failure criterion, whose parameters were determined by Rittel and Brill for commercial PMMA [2], was not previously taken into account in the numerical simulations. The numerical results are based on measured mechanical properties of this material. The calibration of the damage evolution parameter of the ductile failure mode is achieved via simulations of an adiabatic shear band that develops in confined PMMA. Past this preliminary calibration phase, a first test case consists of reproducing the published results of Rosenberg et al. [1]. A second test case consists of simulating new results obtained with a different projectile with a configuration of 3 plates instead of a monolithic one. The numerical results reproduce the observations quite faithfully, with the exception of the damaged (comminuted) zone, for which it is felt that an additional, fracture-

mechanics based, criterion would be helpful, at the risk of complicating the simulations.

The main question was whether the observed ricochet phenomenon could be entirely reproduced using a brittle spalling failure mode, or should a ductile failure mode be introduced for the sake of completeness. The results clearly show that, whereas the ricochet itself is a result of the brittle failure mode, the actual depth of penetration is governed by the combined ductile and brittle failure modes. Including the ductile failure mode provides a more accurate picture of the overall penetration sequence.

Lastly, a new set of data is presented, through a systematic simulation of various impact angles, in order to define a failure envelope for this kind of experiments. In other words, one can now distinguish a range of angles for which the projectile stops (partial penetration), undergoes a ricochet, or simply fully perforates the plate. A detailed characterization of the evolution of the kinetic energy of the projectile is presented both for inclined impact and normal impact. The effect of the projectile's mass and velocity on the DOP was systematically studied, with the main result that the DOP scales linearly with the density at all velocities, with a polynomial dependence on the velocity itself. In addition, it was found that one can devise a sort of universal relationship between the normalized kinetic energy of the projectile and the normalized duration of the penetration process. It is believed that similar systematic investigations might be carried out for other materials, opening the way to reliable simulations of various combinations of materials that are usually considered for protection purposes.

## 8. Conclusions

The conclusions derived from this investigation can be summarized as follows:

- The exact material and failure properties of the PMMA plate are needed to accurately predict a projectile trajectory within it.
- An appropriate plastic displacement damage evolution property for PMMA is fitted by $\bar{u}_f^{pl} = 0.000080\,m$.
- The application of the sole failure criterion "ductile damage with damage evolution" results in a straight trajectory in the impact velocity direction.

- The application of the sole "tensile failure" criterion results in a curved trajectory as a key factor for the observed ricochet phenomenon. Hence the deflection of a projectile from PMMA plates is due to its brittleness (~133 MPa maximum tensile pressure) is in agreement with Rosenberg et al. [1].
- The combined effect of the two failure criteria improves the prediction of the projectile trajectory within the PMMA plate.
- Consequently, numerical simulations can predict the failure envelope of the PMMA plate for a variety of impact angles.
- The loss of kinetic energy during inclined penetration is close to a linear function of time.
- For the parameters used in this investigation, a minimum loss of 50% of the kinetic energy is observed for inclination angles higher than $50^o$ (for which the plate is perforated).
- The DOP scales linearly with the projectile's mass at all investigated impact velocities.
- The DOP can be expressed as a polynomial function of the impact velocity.
- The kinetic energy vaiation with time for normal impact may be approximated by $\frac{E_k}{E_k^i} = f\left(\frac{t}{t_f}\right)$ for various velocities.
- The maximum DOP is quadratic with respect to the impact velocity for the parameters used in this investigation.

**Acknowledgement**

The authors acknowledge the technical assistance and support of the National Ballistic Center at Rafael. This work was supported by the Technion Fund for Security Research.

## References

[1] Z. Rosenberg, Z. Surujon, Y. Yeshurun, Y. Ashuach and E. Dekel**, "** Ricochet of 0.3" AP projectile from inclined polymeric plates", (2005) , *Int. J. Impact Engineering* ,Vol. 31, pp 221–233

[2] D. Rittel and A. Brill, " Dynamic flow and failure of confined polymethylmethacrylate", (2008), *J. Mech. Phys. Solids*, Vol 56/4, pp 1401-1416.

[3] D. Rittel and A. Dorogoy, " A methodology to assess the rate and pressure sensitivity of polymers over a wide range of strain rates", (2008), *J. Mech. Phys. Solids*, 56, 3191-3205.

[4] Abaqus/Explicit Version 6.7-1, Abaqus documentation, Dassault systemes, 2007.

[5] D. Rittel and H. Maigre, "An investigation of dynamic crack initiation in PMMA", *Mechanics of Materials*, (1996), Vol. 23 No. 3, 229-239.

[6] AM. Molodets, and AN. Dremin, "Subcritical stage of cleavage fracture", (1980), Combust..Explos. Shock Waves;16, 545-548.

## TABLES

Table 1 : PMMA properties: Density (ρ), dynamic Young's modulus (E), Poisson's ratio (ν) and frictional Drucker-Prager angle (β) [2].

| property | PMMA |
|---|---|
| ρ [Kg/m$^3$] | 1190 |
| E [GPa] | 5.76 |
| ν | 0.42 |
| $\beta$ [°] | 20 |

Table 2 : Ductile damage initiation properties for PMMA

| Strain rate [1/s] | $\varepsilon_p^{\max}$ | triaxality |
|---|---|---|
| Quasi-static | 0.30 | all |
| 1 | 0.20 | all |
| 2000 | 0.12 | all |
| 4000 | 0.10 | all |
| 40000 | 0.10 | all |

Table 3: Numerical results for DOP

| Vi [m/s] | $\rho_1 = 7800\ [Kg/m^3]$ DOP [mm] | $\rho_2 = 5850\ [Kg/m^3]$ DOP [mm] | $\rho_3 = 3900\ [Kg/m^3]$ DOP [mm] |
|---|---|---|---|
| 200 | 20.6 | 14.7 | 8.8 |
| 300 | 35.3 | 29.4 | 17.6 |
| 400 | 59.1 | 44.1 | 29.4 |
| 500 | 89.4 | 65.2 | 50.0 |
| 600 | 122.7 | 98.5 | 71.2 |
| 720 | - | 125.8 | 89.4 |

Table 4: Coefficients of quadratic approximation

| | a | b | $R^2$ |
|---|---|---|---|
| $\rho_1$ | 0.03942 | 0.0002754 | 0.9991 |
| $\rho_2$ | 0.03596 | 0.0001976 | 0.9946 |
| $\rho_3$ | 0.01796 | 0.0001542 | 0.9896 |

Table 5: ratios between DOP of different densities

| **Vi [m/s]** | $\rho_2/\rho_1$ **= 0.75** | $\rho_3/\rho_1$ **= 0.50** | $\rho_3/\rho_2$ **= 0.67** |
|---|---|---|---|
| 200 | 0.71 | 0.43 | 0.60 |
| 300 | 0.83 | 0.50 | 0.60 |
| 400 | 0.75 | 0.50 | 0.67 |
| 500 | 0.73 | 0.56 | 0.77 |
| 600 | 0.80 | 0.58 | 0.72 |
| 720 | - | - | 0.71 |
| **average** | **0.76** | **0.51** | **0.68** |
| **standard deviation** | 0.05 | 0.05 | 0.06 |

CAPTIONS OF FIGURES

Figure 1: The hardening properties of PMMA for rates $\dot{\varepsilon} = 0.0001$ , 1, 2000, 4000 and 40000 1/s. Note that the higher strain-rate response is assumed to be similar to that measured at 4000 $s^{-1}$.

Figure 2: A typical conical plugs created by adiabatic shear banding of confined PMMA cylinders. (Reprinted from [2]).

Figure 3: Contour maps of the equivalent plastic strain at time 51, 55 and 59 $\mu s$ showing the evolution of the damage which creates a conical plug similar to that shown in figure 2, thus validating the choice of the damage parameter, $\bar{u}_f^{pl} = 80\,\mu m$ . $\bar{u}_f^{pl} = 80\,\mu m$ . A velocity of 25 m/s was applied to the upper face.

Figure 4: a. A typical 0.3" projectile. b. Same projectile impacting a PMMA plate of $250 \times 80 \times 50$ *mm* at an angle of inclination $\alpha = 30^\circ$ .

Figure 5: A detail showing the mesh of the projectile and the plate.

Figure 6: Trajectories of the 0.3" projectile in a PMMA plate. a. numerical results. b. experimental results (Reprinted from [1]). Note the similarity between the numerical simulation and the experimental observation of the projectile's ricochet.

Figure 7: a. The 0.5" projectile. b. An 0.5" projectile impacting 3 PMMA plates at an angle of inclination $\alpha = 30^\circ$ .

Figure 8: a. The meshed geometry. b. A detail of the projectile mesh.

Figure 9: A 0.5" projectile impact on three PMMA plates at a $30^\circ$ angle of inclination and 928 m/s impact velocity. Note the ricochet of the projectile.

Figure 10: Trajectories of the projectile and the damaged PMMA plates at three different times which correspond to time intervals of 220 μs and 200 μs of the experimental results shown in figure 9:. a. 80.μs, b. 300 μs, c. 500 μs.

Figure 11: Trajectories of the projectile due the usage of different failure criteria. a. ductile failure – no ricochet. b. tensile failure – modest penetration followed by ricochet.

Figure 12: Trajectories of a 0.3" steel projectile impacting a PMMA plate at different angles of inclination ($10^o$ ,. $20^o$,. $40^o$ ,. $50^o$ , $60^o$, $70^o$ , $80^o$ and $90^o$). The weight is 5.8 gr and the impact velocity 720 m/s. Results for $30^o$ are shown in figure 6a.

Figure 13: Time evolution of the normalized kinetic energies of the projectile for different angles of inclination impacting with a speed of 720 m/s.

Figure 14: The plate model showing the DOP of 0.3" projectile impacting a

thick PMMA plate at 600 m/s.

Figure 15: The DOP vs. impact velocity for normal penetration in PMMA for three different projectile densities: $\rho_1$ = 7800, $\rho_2$ = 5850 and $\rho_3$ = 3900 $\left[Kg/m^3\right]$.

Figure 16: Variation of the kinetic energy of the projectile with time for impact velocities: 200, 300, 400, 500, 600 and 720 m/s as well as two different densities: $\rho$=7800 and 3900 [Kg/m$^3$]. a: Real values for velocity for $\rho$=7800 [Kg/m$^3$] . b. Normalized values for $\rho$=7800 [Kg/m$^3$] . c. Real values for $\rho$=3900 [Kg/m$^3$] . d. Normalized values for $\rho$=3900 [Kg/m$^3$].

FIGURES

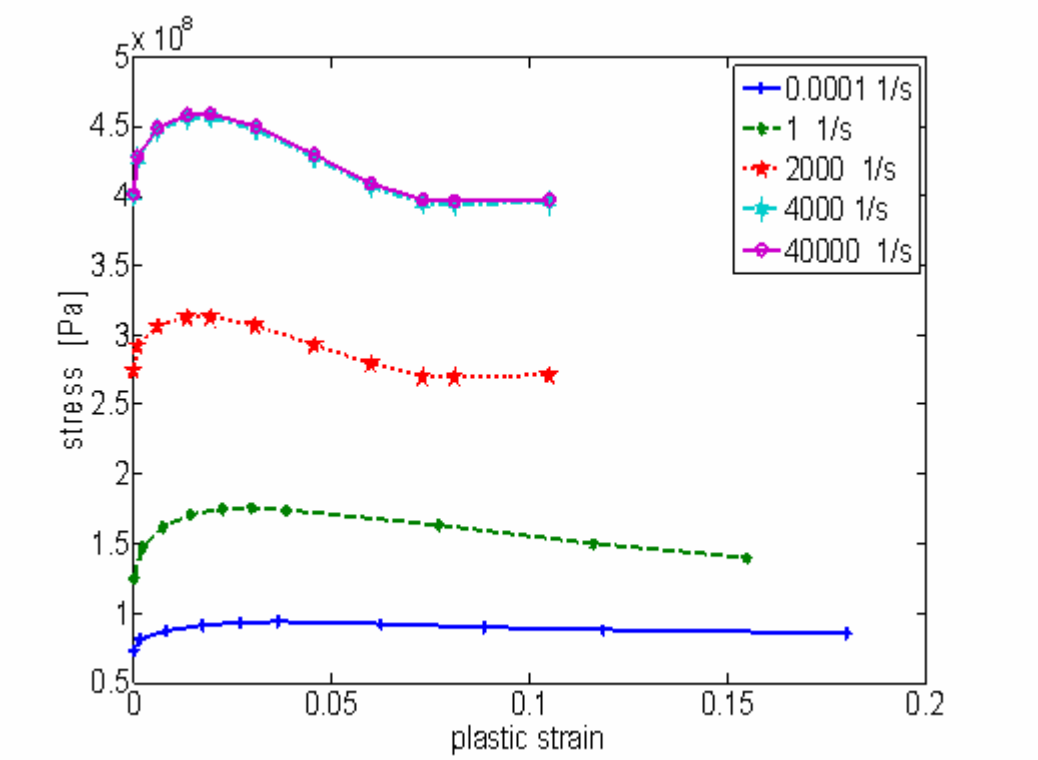


Figure 1: The hardening properties of PMMA for rates $\dot{\varepsilon} = 0.0001$ , 1, 2000, 4000 and 40000 1/s. Note that the higher strain-rate response is assumed to be similar to that measured at 4000 $s^{-1}$.

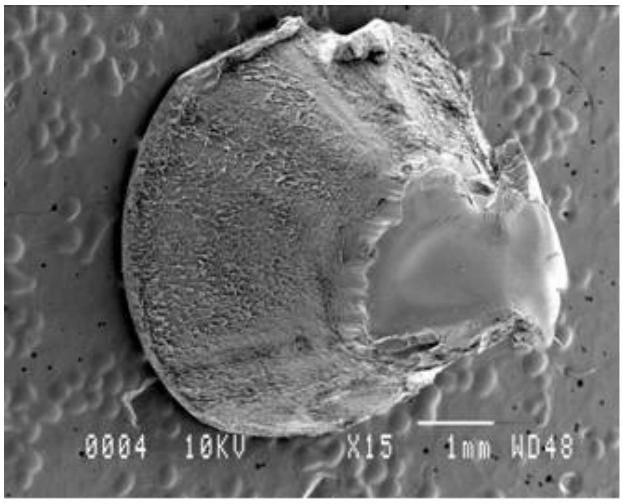


Figure 2: A typical conical plugs created by adiabatic shear banding of confined PMMA cylinders. (Reprinted from [2]).

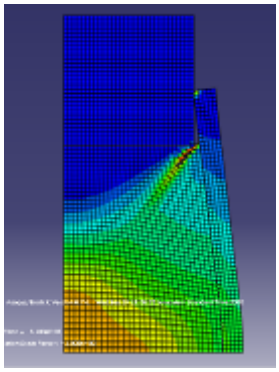

a.

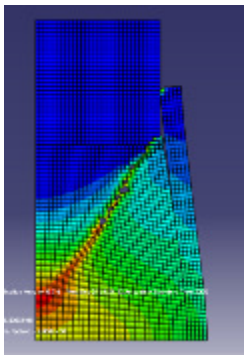

b.

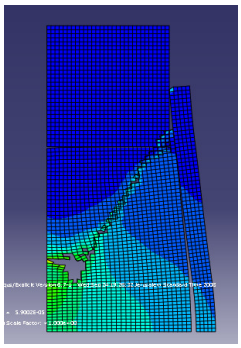

c.

Figure 3: Contour maps of the equivalent plastic strain at time 51, 55 and 59 $\mu s$ showing the evolution of the damage which creates a conical plug similar to that shown in figure 2, thus validating the choice of the damage parameter, $\overline{u}_f^{pl} = 80\,\mu m$. A velocity of 25 m/s was applied to the upper face.

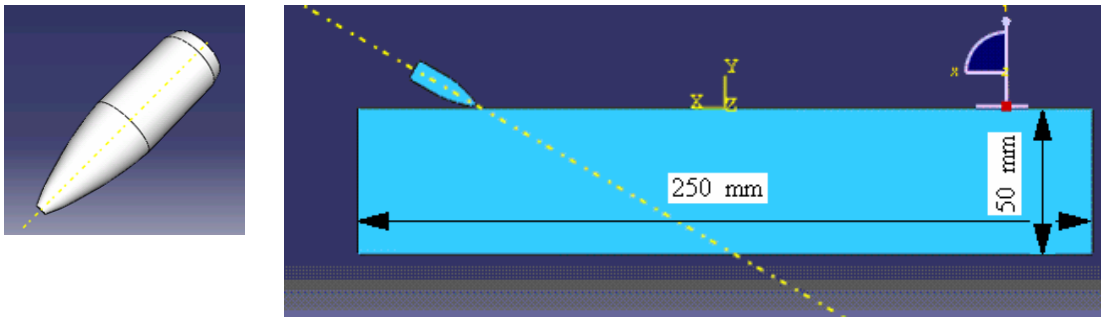


a. b.

Figure 4: a. A typical 0.3” projectile. b. Same projectile impacting a PMMA plate of $250\times80\times50$ *mm* at an angle of inclination $\alpha=30^{\circ}$.

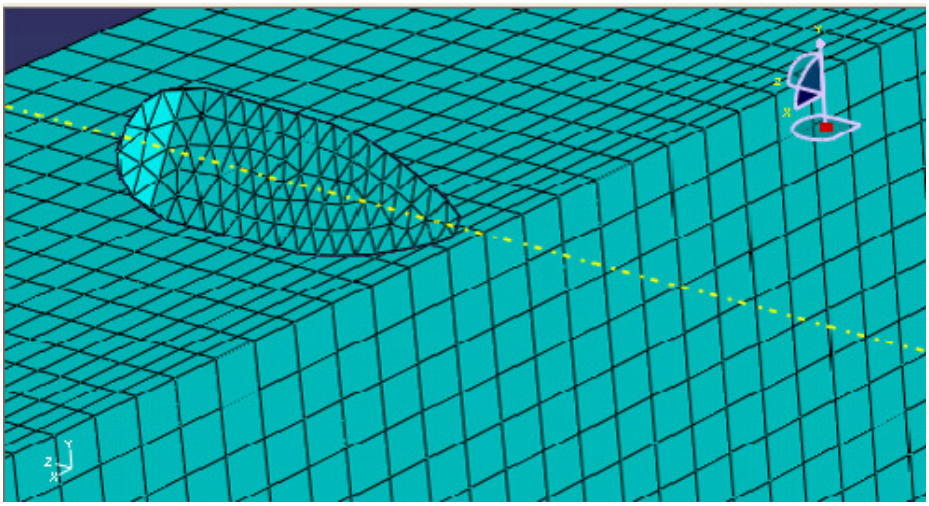

Figure 5: A detail showing the mesh of the projectile and the plate.

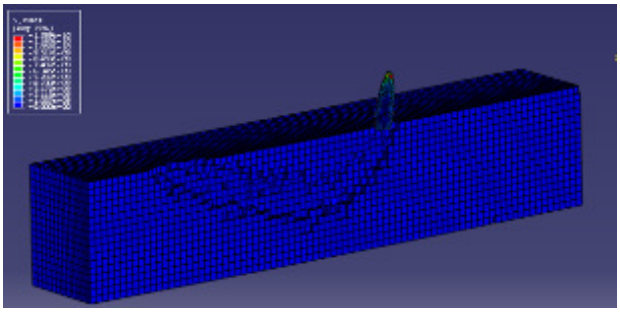

a.

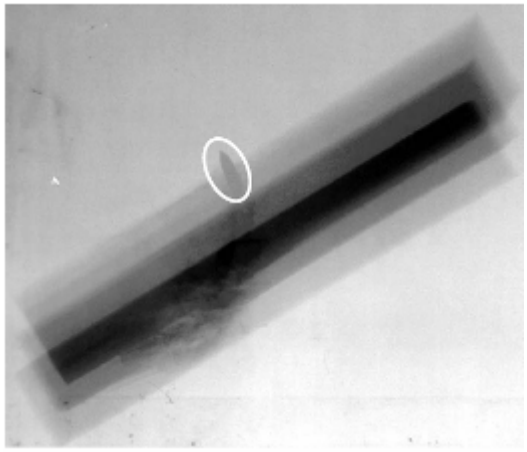

b.

Figure 6: Trajectories of the 0.3" projectile in a PMMA plate. a. numerical results. b. experimental results (Reprinted from [1]). Note the similarity between the numerical simulation and the experimental observation of the projectile's ricochet.

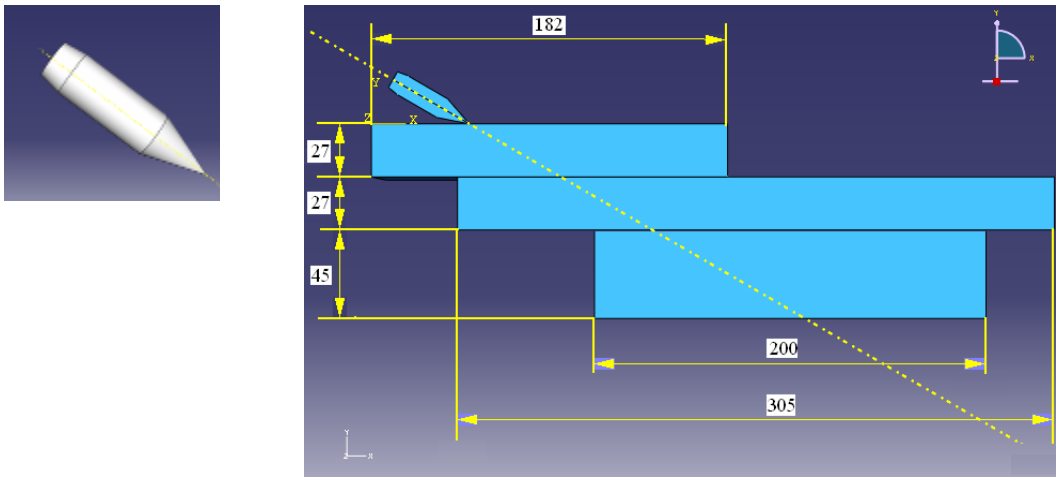


a. b.

Figure 7: a. The 0.5" projectile. b. An 0.5" projectile impacting 3 PMMA plates at an angle of inclination $\alpha = 30^{\circ}$.

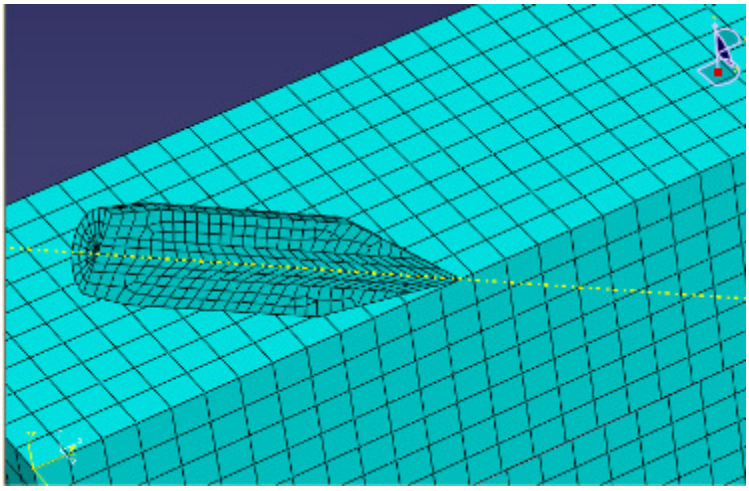

Figure 8: a. The meshed geometry. b. A detail of the projectile mesh.

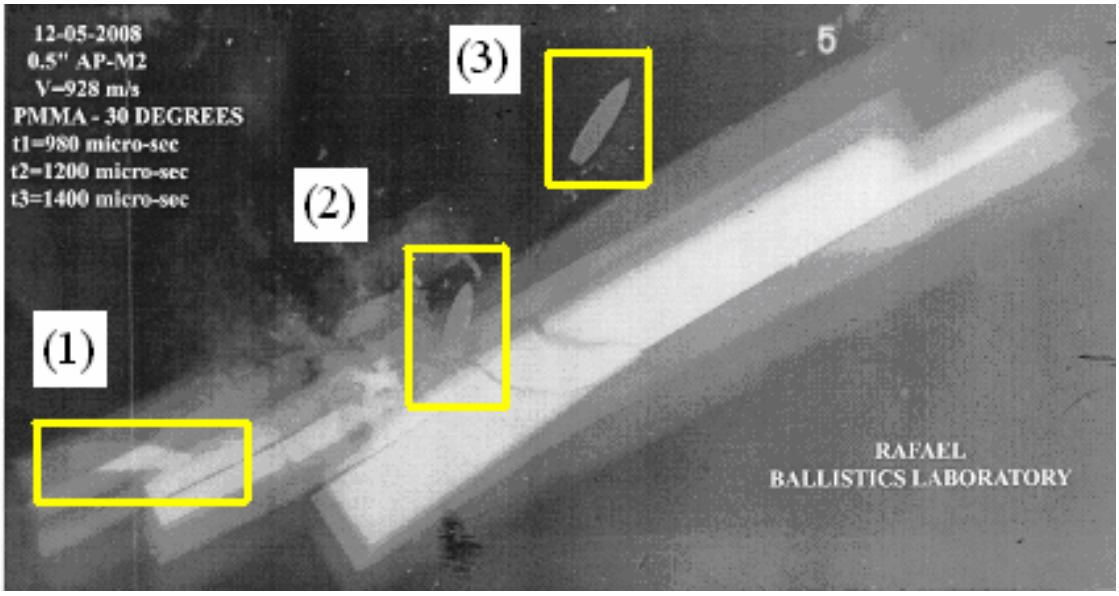


Figure 9: A 0.5" projectile impact on three PMMA plates at a $30^{\circ}$ angle of inclination and 928 m/s impact velocity. Note the ricochet of the projectile.

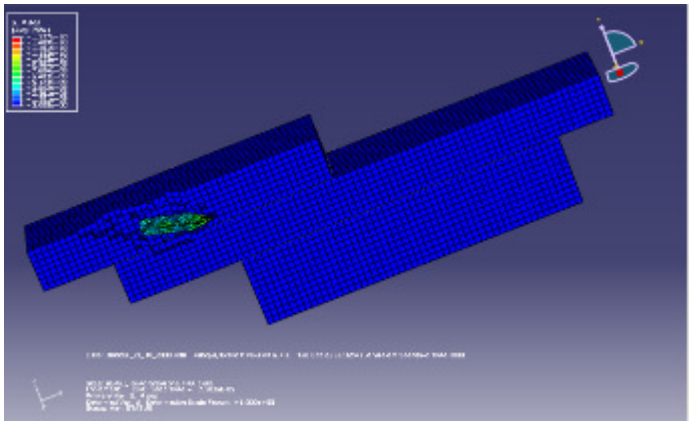

a.

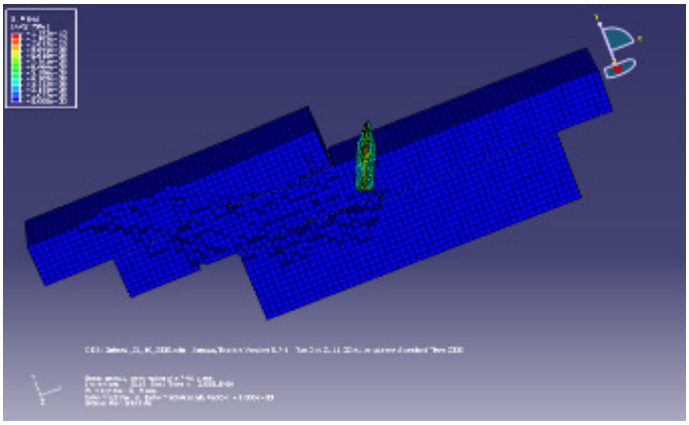

b.

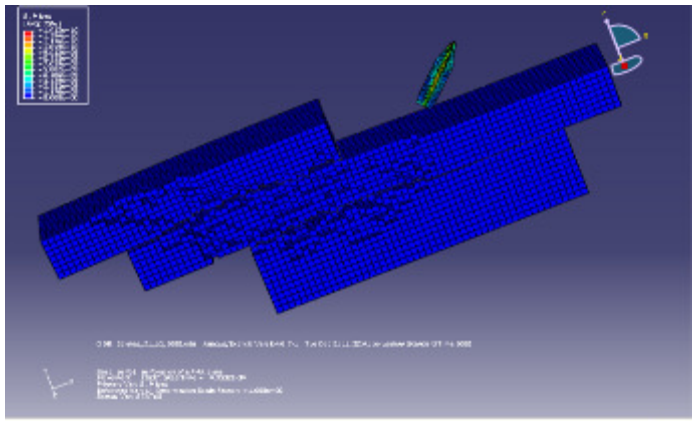

c.

Figure 10: Trajectories of the projectile and the damaged PMMA plates at three different times which correspond to time intervals of 220 μs and 200 μs of the experimental results shown in figure 9:. a. 80.μs, b. 300 μs, c. 500 μs.

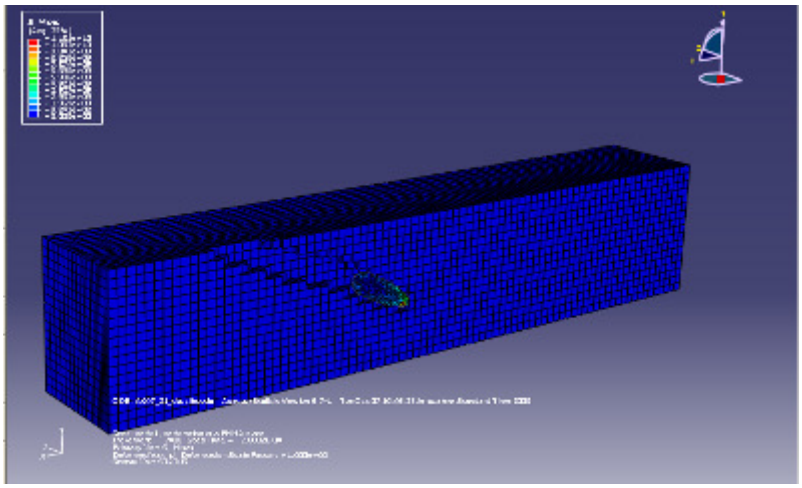

a.

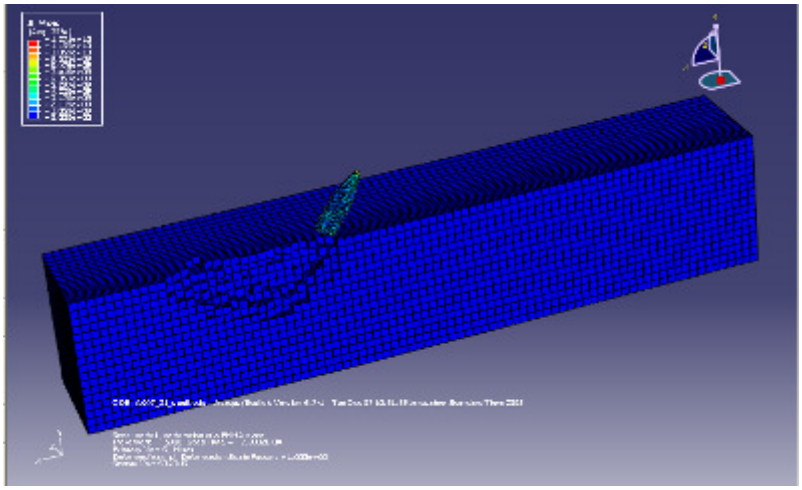

b.

Figure 11: Trajectories of the projectile due the usage of different failure criteria. a. ductile failure – no ricochet. b. tensile failure – modest penetration followed by ricochet.

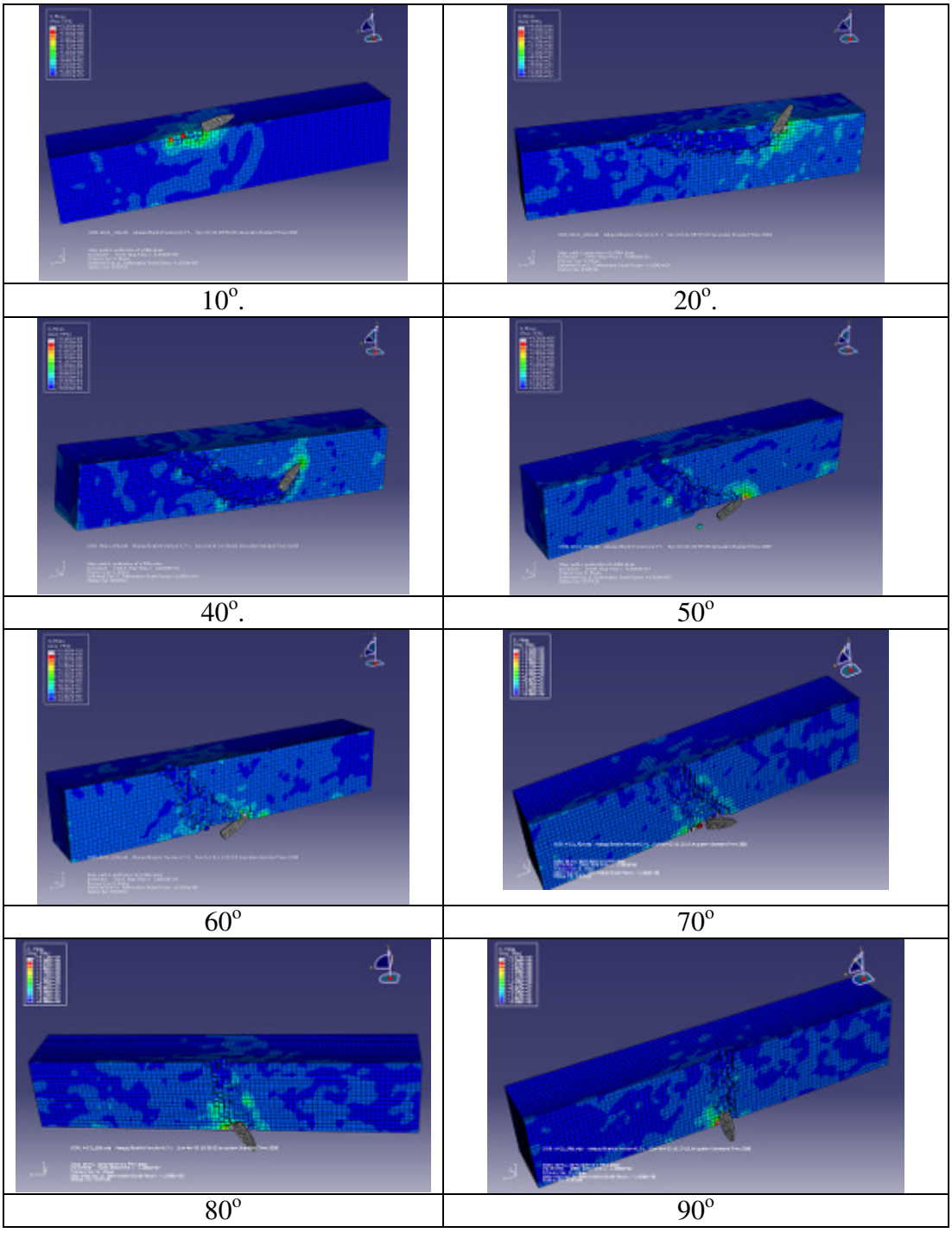


Figure 12: Trajectories of a 0.3" steel projectile impacting a PMMA plate at different angles of inclination ($10^o$ ,. $20^o$,. $40^o$ ,. $50^o$ , $60^o$, $70^o$ , $80^o$ and $90^o$). The weight is 5.8 gr and the impact velocity 720 m/s. Results for $30^o$ are shown in figure 6a.

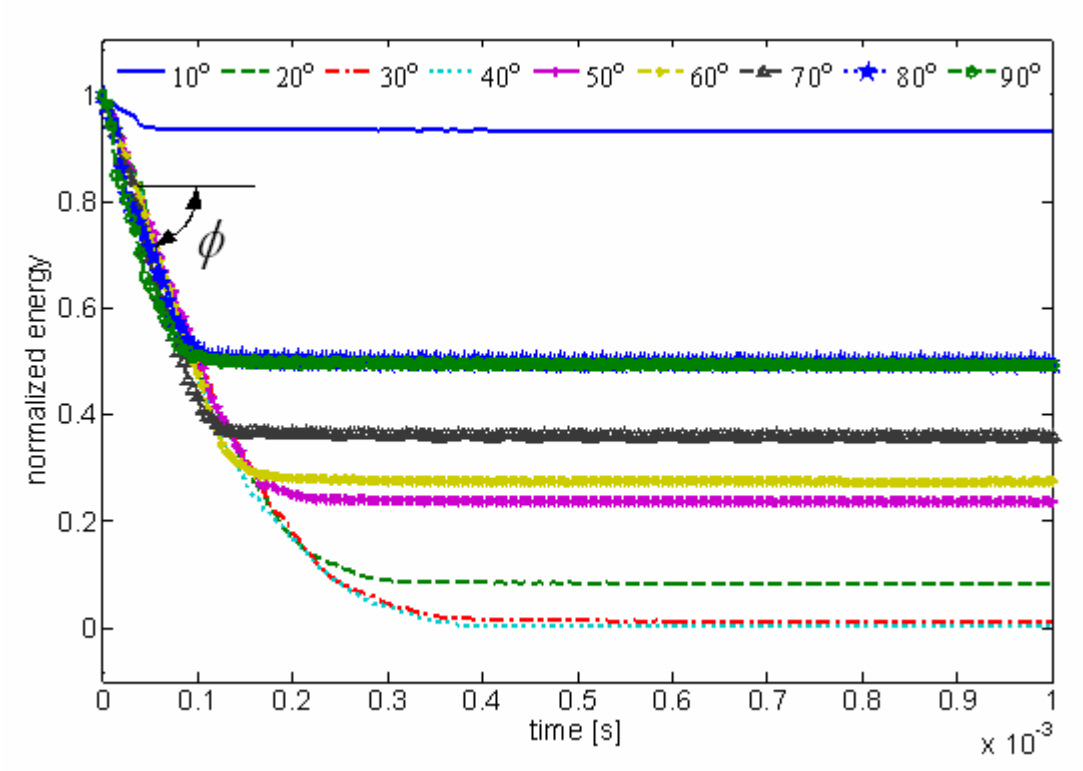


Figure 13: Time evolution of the normalized kinetic energies of the projectile for different angles of inclination impacting with a speed of 720 m/s.

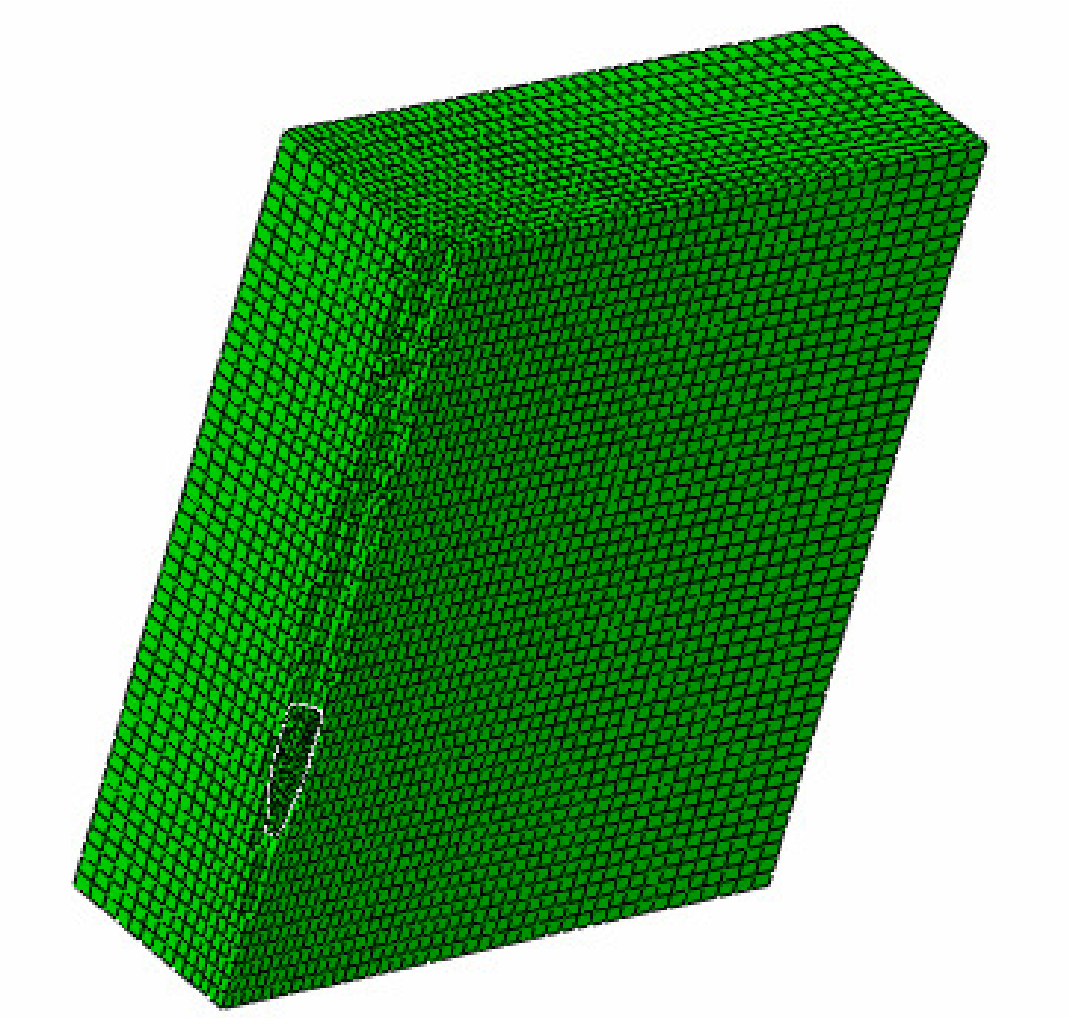

Figure 14: The plate model showing the DOP of 0.3" projectile impacting a thick PMMA plate at 600 m/s.

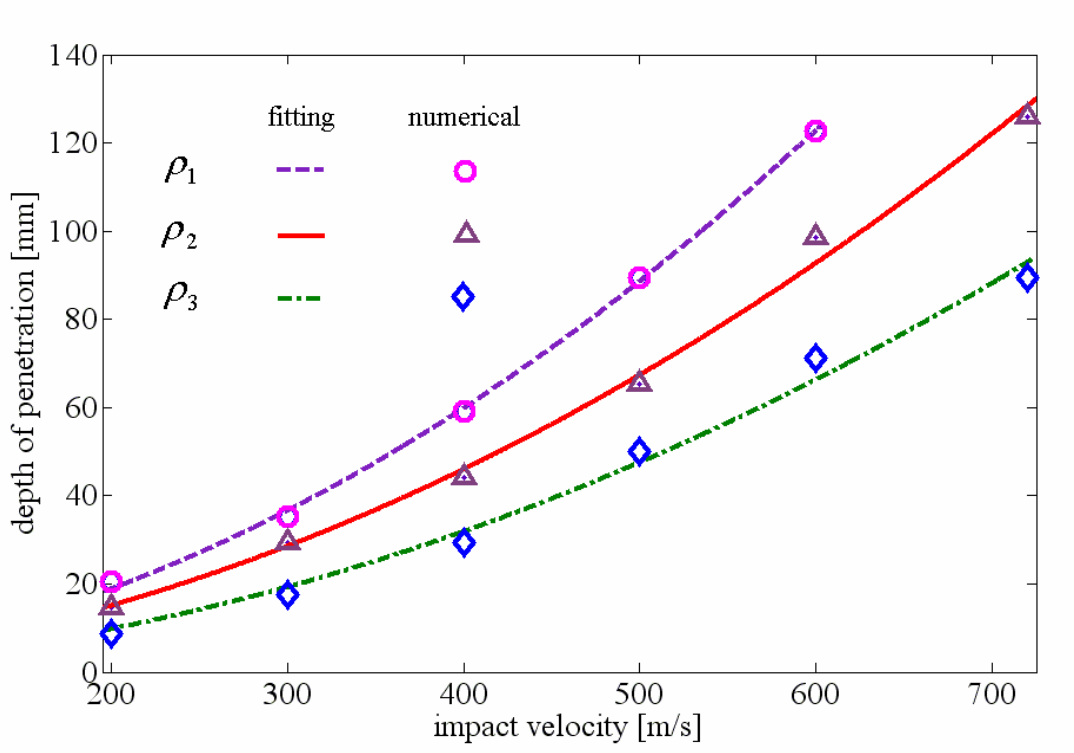


Figure 15: The DOP vs. impact velocity for normal penetration in PMMA for three different projectile densities: $\rho_1 = 7800$, $\rho_2 = 5850$ and $\rho_3 = 3900$ $\left[Kg / m^3\right]$.

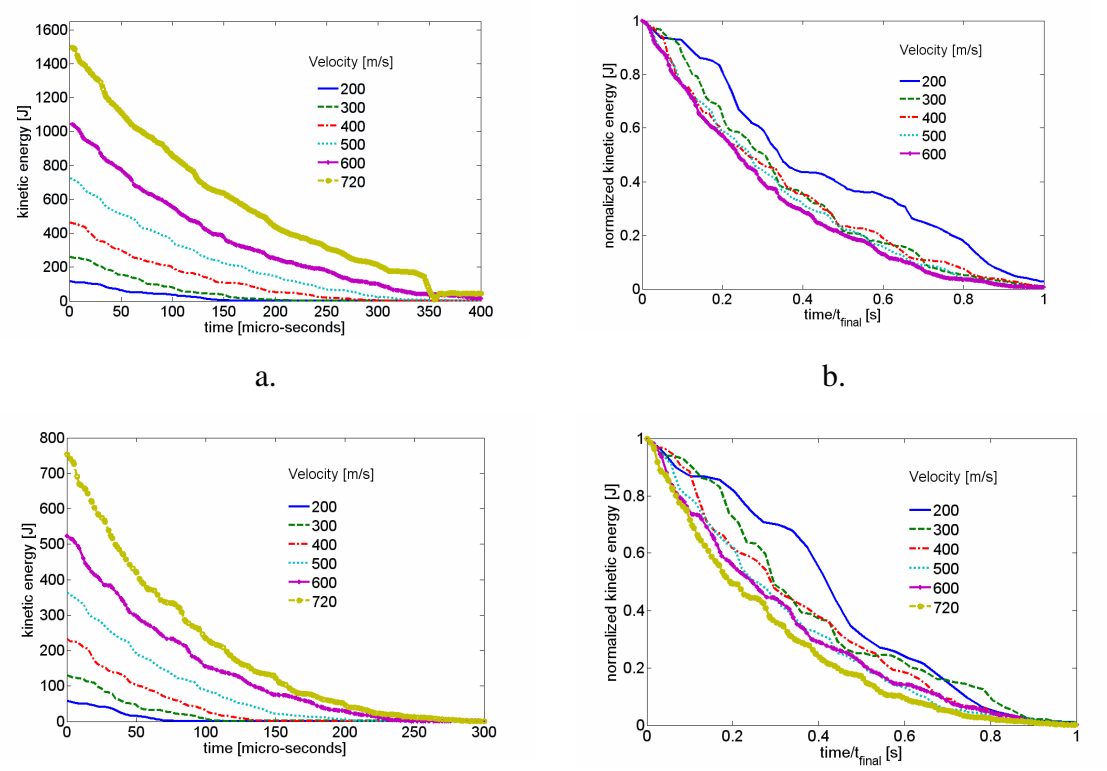


Figure 16: Variation of the kinetic energy of the projectile with time for impact velocities: 200, 300, 400, 500, 600 and 720 m/s as well as two different densities: $\rho$=7800 and 3900 [Kg/m$^3$]. a: Real values for velocity for $\rho$=7800 [Kg/m$^3$] . b. Normalized values for $\rho$=7800 [Kg/m$^3$] . c. Real values for $\rho$=3900 [Kg/m$^3$] . d. Normalized values for $\rho$=3900 [Kg/m$^3$].

.